Journal of Molecular Liquids 255 (2018) 122–134

Contents lists available at ScienceDirect

Journal of Molecular Liquids

journal homepage: www.elsevier.com/locate/molliq

Synthesis and characterization of ruthenium(III) complex containing 2-aminomethyl benzimidazole, and its anticancer activity of *in vitro* and *in vivo* models

H.A. Sahyon [a], A.A. El-Bindary [b,*], A.F. Shoair [b,c], A.A. Abdellatif [b]

[a] Chemistry Department, Faculty of Science, Kafrelsheikh University, Kafrelsheikh, 33516, Egypt
[b] Chemistry Department, Faculty of Science, Damietta University, Damietta 34517, Egypt
[c] Chemistry Department, Faculty of Science, Taif University, Taif, Saudi Arabia

ARTICLE INFO

Article history:
Received 7 December 2017
Received in revised form 23 January 2018
Accepted 24 January 2018
Available online xxxx

Keywords:
Ru(III) complex
2-Aminomethyl benzimidazole
MTT, anticancer
CT-DNA
Top I

ABSTRACT

A novel ruthenium(III) complex with 2-aminomethyl benzimidazole (AMBI) has been synthesized and characterized by elemental analysis, spectroscopic (FTIR, UV–Vis and XRD), thermal, magnetic and electrochemical techniques. Characterization shown that the ruthenium ion is octahedral coordinated by three H_2O molecules, one chloride ion and a bidentate AMBI. The calf thymus DNA binding activity of complex was studied by absorption spectra and viscosity measurements. The strong interaction between Ru(III) complex and CT-DNA was investigated and the K_b value equals 8.3×10^{-5}. The cytotoxicity effect of water soluble $[RuCl(AMBI)(H_2O)_3]Cl_2$ complex on breast adenocarcinoma (MCF-7) and human colon carcinoma (HCT-116) cell lines (*in vitro*) was investigated by the MTT method. The Ru(III) complex shows good cytotoxic activity and the IC_{50} values are 57.20 and 18.08 μg/mL toward MCF-7 and HCT-116, respectively. The antiproliferative effect of Ru(III) complex on HCT-116 cells was nearly as the cisplatin value; that indicates its efficiency as anticancer agents. Apoptosis was studied by AO/EB staining and the Ru(III) complex shows apoptotic effect against the two cancer cell lines by percent to 23.1 and 33.1%. DNA damage assay by gel electrophoresis was done and the DNA fragmentation that appears in the two treated lanes indicates that there was destruction in the nuclear DNA. The cell cycle arrest by flow cytometry showed that the Ru(III) complex stops the two cancer cell lines proliferation by decrease the S and G0/G1 phases and increase in G2/M indicates that the interactions of our complex with DNA prevents the entry of cells into the DNA synthesis phase as well as into a new cell cycle. Moreover, the Ru(III) complex stops the proliferation of Ehrlich ascites carcinoma (EAC) bearing female mice (*in vivo* study) with low toxicity to the kidney. In addition, the antioxidant enzymes' activity in the treated and untreated groups' blood samples were also investigated. The decrease in topoisomerase I (*Top I*) levels in treated mice groups than the EAC group indicates the effect of our compound as topoisomerase I inhibitor.

1. Introduction

Cancer is a devastating disease that strikes different people all over the world. Breast cancer is the most second common cancer worldwide after lung cancer [1]. Delay screening with late diagnosis of breast cancer leads to metastasis all over the body causing death [2]. Cisplatin is used clinically in the treatment of a variety of cancers; but with long times of treatment, it causes nephrotoxicity, hepatotoxicity and drug resistance [3]. These side effects encourage the scientists to invent new anticancer drugs with less toxicity like ruthenium complexes. The new anticancer drugs based on ruthenium metal take large attention because the coordination and redox properties of ruthenium metal [4]. Chemical properties of ruthenium metal make it a promising anticancer drug to be used as a core with certain ligand complexes [5]. Recent studies have used Ru(III) complexes as an anticancer drug against different human cell lines (*in vitro*) with a great bioactivity of these complexes [6,7]. Unlike cisplatin; the *in vivo* studies of ruthenium complexes proved that they have minimal kidney toxicity that can be reversed after quitting [8]. Minor number of Ru(III) complexes get into pre-clinical trials [9,10] as an anti-breast cancer [11,12], but still there was a lack in *in vivo* studies with the development of safer, water soluble Ru(III) complexes.

Benzimidazoles ligand has the structure similar to purine base of the DNA and the nucleus of vitamin B12 [13]. That similarity allows the biological systems to recognize the benzimidazole ring without any sign of allergy [14]. Also, it shows anti-inflammatory, DNA cleaving properties and anticancer activities against various cancer cell lines alone and

* Corresponding author.
E-mail address: abindary@yahoo.com (A.A. El-Bindary).

https://doi.org/10.1016/j.molliq.2018.01.140
0167-7322/

with metal chelators such as ruthenium(I), iron(II), platinum(II) and zinc(II) [15–17]. Benzimidazole compounds were also reported as topoisomerase I, tyrosine kinase and serine protease inhibitors [18]. Different complexes of transition metals with 2-substituted benzimidazole were proven to be effective as anticancer [19]. Some benzimidazole derivatives show diverse biological activities in the treatment of leukemia and cancer. In addition, the stability of the 2-aminomethyl benzimidazole due to aromatic ring π-π stacking effects made it promising to be the choice ligand for ruthenium(III). The innovation of new anticancer drug design with special properties is currently needed in clinical fields. Therefore, this study aimed to synthesize a safe and effective anticancer drug with ruthenium core by selecting a heterocyclic ligand with known safety and anticancer activity like the benzimidazoles ring structure. The calf thymus DNA binding activity of water soluble $[RuCl(AMBI)(H_2O)_3]Cl_2$ complex was studied by absorption spectra and viscosity measurements. MCF-7 cells (breast adenocarcinoma) are considered a violent drug resistant cancer cells. The chemotherapeutic drug that can affect these cells will consider a potent anticancer. Thus, we examine the cytotoxic effect of our complex on MCF-7 as well as on HCT-116 (human colon carcinoma) cell lines (*in vitro*). Then, we study the apoptotic analysis and cell cycle arrest of our complex on the treated cell lines. Besides its effect on Ehrlich ascites carcinoma (EAC) transplanted in female mice as a mammary adenocarcinoma model (*in vivo* study) with the toxicity profile of this complex on different mice organs in treated and healthy mice. Finally, the topoisomerase I level was determined in all mice groups.

2. Materials and methods

2.1. Chemicals and reagents

Hydrated ruthenium trichloride ($RuCl_3 \cdot 3H_2O$/10452), 2-aminomethyl benzimidazole dihydrochloride (AMBI/165638), tetrabutylammonium hexafluorophosphate (TBHFP/281026), acridine orange (AO/A6014) and ethidium bromide (EB/E7637) were obtained from Sigma-Aldrich and used without further purification. Other chemicals and solvents were obtained from Fluka and used as received. Serum glutamate-pyruvate transaminase (SGPT), serum glutamate-oxaloacetate transaminase (SGOT), albumin, total bilirubin, creatinin, urea and uric acid kits were from Spinreact, Spain. Super oxide dismutase (SOD) kit, malondialdehyde (MDA) kit, reduced glutathione (GSH), catalase (CAT) and total antioxidant capacıty (TAC) kits were from Biodiagnostic, Egypt. Hemoglobin kit was from Randox Laboratory Ltd., UK. White blood cells count reagent was from Egyptian Diagnostic Media Co., Egypt.

2.2. Instrumentation

Microanalytical data (C, H and N) were collected on Automatic Analyzer CHNS Vario ELIII, Germany. Infrared spectra (KBr discs, 4000–400 cm^{-1}) were recorded on Jasco FTIR-4100 spectrophotometer. UV–Visible spectra were recorded by Perkin-Elmer AA800 spectrophotometer Model AAS. Fluorescence microscopy BK6000, China. Magnetic susceptibility measurements were determined at room temperature on a Johnson Matthey magnetic susceptibility balance using $Hg[Co(SCN)_4]$ as calibrant. X-ray diffraction analysis of compound in powder forms were recorded on X-ray diffractometer in the range of diffraction angle $2\theta = 10–80°$. This analysis was carried out using CuKα radiation ($\lambda = 1.540598$ Å). The applied voltage and the tube current are 40 kV and 30 mA, respectively. Scherer's equation [20] calculates the average crystallite size, t, using the Eq.: $t = 0.95\lambda\ \gamma/\cos\ \Theta$, where γ is the width measured in radians of the half-maximum peak intensity, λ is the X-ray wavelength and Θ is the Bragg's angle. Thermal analysis of $[RuCl(AMBI)(H_2O)_3]Cl_2$ complex was carried out using a Shimadzu thermogravimetric analyzer under a nitrogen atmosphere with heating rate of 20 °C/min over a temperature range from room temperature up to 1000 °C. Conductivity measurements of the complex at 25 ± 1 °C were determined in water (10^{-3} M) using conductivity/TDS meter model Lutron YK-22CT. The electrochemical behavior of the complex was studied using an electrochemical analyzer CHI 610A (HCH Instrument) under nitrogen atmosphere and at room temperature. The electrochemical cell that was used in this work contains three electrodes: platinum wire was used as a working electrode, Ag^+/AgCl was used as a reference electrode and a platinum wire was used as a counter electrode.

2.3. Synthesis of $[RuCl(AMBI)(H_2O)_3]Cl_2$ complex

2-aminomethyl benzimidazole (0.440 g, 2 mmol) was dissolved in 20 cm^3 of ethanol. $RuCl_3 \cdot 3H_2O$ (0.261 g, 1 mmol) was dissolved and refluxed in ethanol (20 cm^3) until the initial black color turned into green. The aqueous of the ligand previously prepared was added to this green solution, then the reaction mixture was refluxed for 3 h. As a result of refluxing green microcrystals was formed which were collected by filtration using filtered glass gooch, washed with ethanol (10 cm^3) and dried in a vacuum desiccator over anhydrous $CaCl_2$. The analytical data for that complex are well agreed with its formula. Anal. Calcd. for $C_8H_{15}Cl_3N_3O_3Ru$ (%): C, 23.91; H, 3.73; N, 10.70. Found (%): C, 23.71; H, 3.70; N, 10.55.

$$RuCl_3 \cdot 3H_2O + AMBI \rightarrow [RuCl(AMBI)(H_2O)_3]Cl_2$$

2.4. DNA binding

The binding properties of complex to calf thymus DNA have been studied using electronic absorption spectroscopy. The stock solution of CT-DNA was prepared in (1×10^{-3} M) Tris–HCl/50 mM NaCl buffer (pH 7.2), which a ratio of UV absorbances at 260 and 280 nm (A_{260}/A_{280}) of CT-DNA 1.8–1.9, indicating that the DNA was sufficiently free of protein [21], and the concentration was determined by UV absorbance at 260 nm ($\varepsilon = 6600\ M^{-1}\ cm^{-1}$) [22]. Electronic absorption spectra (200–700 nm) were carried out using 1 cm quartz cuvettes at 25 °C by fixing the concentration of complex (3×10^{-4} M), while gradually increasing the concentration of CT-DNA (0.00–1.15×10^{-4} M). An equal amount of CT-DNA was added to both the complex solutions and the references buffer solution to eliminate the absorbance of CT-DNA itself. The intrinsic binding constant K_b of the complex with CT-DNA was determined using Eq. (1) [23]:

$$[DNA]/(\varepsilon_a - \varepsilon_f) = [DNA]/(\varepsilon_b - \varepsilon_f) + 1/K_b(\varepsilon_a - \varepsilon_f) \quad (1)$$

where [DNA] is the concentration of CT-DNA in base pairs, ε_a is the extinction coefficient observed for the A_{obs}/[complex] at the given DNA concentration, ε_f is the extinction coefficient of the free complex in solution and ε_b is the extinction coefficient of the complex when fully bond to DNA. In plots of [DNA]/($\varepsilon_a - \varepsilon_f$) *vs.* [DNA], K_b is given by the ratio of the slope to the intercept.

2.5. Viscosity measurements

Viscosity measurements were performed at compound concentration within the range of ($0.1–1 \times 10^{-3}$ M) and each compound was added into a DNA solution (1×10^{-3} M) present in the viscometer. The average flow times of three replicates were measured with a digital stopwatch. The data were presented as $(\eta/\eta_o)^{1/3}$ *vs.* [complex]/[DNA] ratio of the concentration of the compound to DNA [24], where η and η_o are the viscosity of the DNA in the presence and absence of complex, respectively [25]. The relative viscosities η were calculated using Eq. (2) [26]:

$$\eta = (t - t_o)/t_o \quad (2)$$

where t is the observed flow time of DNA containing solution and t_o is the flow time of buffer alone.

2.6. Measurement of cytotoxic activity by MTT assay

Human colon carcinoma (HCT-116) and breast adenocarcinoma (MCF-7) cells were purchased from American Type Culture Collection (ATCC, NY, USA). The cells were seeded at a density of 1×10^4 cells per well (100 μL/well) onto 96-well plate (Falcon, Franklin Likes, NJ) in DMEM medium (GIBCO, Grand Island, New York, USA; Cat.no. A1049101). Ru(III) complex was added with different concentrations (5, 8, 10, 40, 80 and100 μg/mL) for 24 h at 37 °C in a 5% CO_2 with 95% humidity incubator and compared with different concentrations of cisplatin as reference chemotherapeutic drug (3.125, 6.25, 12.5, 25, 50 and 100 μg/mL). The medium was washed gently twice with ice-cold PBS and a volume of 200 μL MTT [3-(4,5-Dimethylthiazol-2-yl)-2,5-diphenyltetrazolium bromide, a yellow tetrazole, (Molecular probes, Eugene, Oregon, USA; Cat. No. V-13154)] was added to each well. After several steps, the absorbance of each well was measured at 630 nm using a microplate reader (ELX800, Biokit, Spain). The cell inhibition percentage was calculated using Eq. (3):

$$\%\text{Cell viability} = [(A_t - A_b)/(A_c - A_b)] \times 100 \quad (3)$$

where, A_t = Absorbance value of tested compound; A_b = Absorbance value of blank; A_c = Absorbance value of control; and % Cell inhibition = 100 − cell viability.

Assays were performed in triplicate on three independent experiments. The concentration of Ru(III) complex inhibiting 50% of cells (IC_{50}) was calculated using the sigmoidal curve that was plotted between the sample concentration and the % cell viability.

2.7. Fluorescence analysis of apoptosis and necrosis in living cells

The mode of cell death was determined by investigating apoptosis and necrosis ratios using double stain with acridine orange/ethidium bromide (AO/EB) according to the method of Ribble et al. [27]. Briefly, AO/EB staining is used to visualize nuclear changes and apoptotic body formation that is exact representative of apoptosis. AO is a dye that is nucleic acid selective fluorescent cationic membrane-permeable that will stain all the viable cells and appear the nuclei in green color. EB is a dye that is taken up by the necrotic cells because cytoplasmic membrane integrity is lost, and stains the nucleus with red color. Thus, live cells have a normal green nucleus; early apoptotic cells have bright green to yellow nucleus; late apoptotic cells show fragmented orange chromatin and cells have died from direct necrosis have a dark orange to red nucleus.

Cancer cell lines were cultured in six well plates at a density of 5×10^5 cells/well and treated for 24 h with 30% of the IC_{50} value of the Ru (III) complex then incubated at 37 °C in a humidified 5% CO_2 atmosphere. Finally, cells were removed by trypsinization and resuspended in 50 μL PBS and 2 μL of a solution containing 100 μg/mL AO and 100 μg/mL EB in PBS was added. Stained cell suspension (10 μL) was placed on a clean microscope slide and covered with a coverslip. Cells were visualized and counted by fluorescence microscopy. For each cell line, three treated wells and three untreated wells were examined, and the mean cells count was calculated. For each sample, at least 500 cells were counted, and the percentage of apoptotic or necrotic cells was determined (Eq. (4)):

$$\%\text{of apoptotic or necrotic} = (\text{the total number of apoptotic or necrotic cells}/\text{total number of cells counted}) \times 100. \quad (4)$$

2.8. DNA damage assay

The DNA extraction was done by DNA Extraction Kit (Fermentas, #K0721, European Union). The genomic DNA was extracted using Gene JET genomic DNA extraction kit following the manufacturer protocol (Fermentas, #K0721, European Union). Simply, in this method the DNA cells extract from different cell lines after incubation with the IC_{50} value of Ru(III) complex for 24 h were loaded in an agarose gel well in the presence of DNA molecular weight marker (ladder) in the adjacent well. Then the gel electrophoresis was done for 2 h. The fragment patterns (ladder, smear or intact) were visualized on the UV Trans-illuminator and photographed by gel documentation system (UVDI Major Science, USA).

2.9. Investigation of cell cycle arrest by flow cytometry

Briefly, two six-well plates were seeded with MCF-7 and HCT-116 cells respectively at a density of 2×10^5 cells per well. The cells were cultured in RPMI 1640 supplemented with sterile-filtered fetal bovine serum (FBS) 10% and were incubated at 37 °C and 5% CO_2 for 24 h. The medium was removed and replaced with medium (final bi-distilled water concentration, 0.05% v/v) containing IC_{50} of the complex into three wells for every cell line and the other three wells remain untreated as control wells. After incubation for 24 h, the cell layer was trypsinized and washed with cold PBS and fixed with 70% ethanol which added drop wise to the wells. Then, fixed for 30 min at 4 °C after that, 20 μL of RNase (0.2 mg/mL) and 20 μL of propidium iodide (0.02 mg/mL) were added to the cell suspensions and they were incubated at 37 °C for 30 min. Then the treated and untreated cell samples were analyzed in triplicated manner with Attune, Applied Biosystems, USA, flow cytometry system. The number of cells analyzed for each sample was 10,000. The flow cytometric software used an algorithm which attempt to fit Gaussian curves to each phase with a calculated percentage.

2.10. Animal experiments

In the department animal house, the female albino mice aged 6–7 weeks old, average weigh 22–24 g, were used. The animals were fed a standard pellet diet and water *ad libitum*. Housed in a polypropylene cage with a 12 h light and dark cycle at room temperature. Animal's procedures were approved and maintained in accordance with the guidelines of the Animal Ethical Committee of Kafrelsheikh University, Egypt.

2.10.1. Median lethal dose (LD_{50}) determination

The tested compounds were dissolved in warm sterile distilled water for injection and vortex till solution clarity, then injected intraperitoneally to seven groups of mice (each containing four mice) at different doses (10, 20, 40, 50, 100, 150 and 200 mg/kg). LD_{50} was estimated by recording mortality after 24 h.

It was found that the LD_{50} value was 200 mg/kg. The mice maximum tolerated dose was 50 mg/kg of Ru(III) complex (1/4 of LD_{50}) from day 1 to day 7 without any weight loss or signs of toxicity. We use this dose as the high dose in our experiment besides the low dose 25 mg/kg of Ru (III) complex.

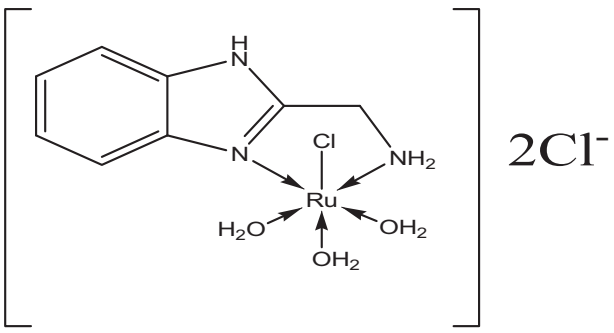

Fig. 1. The proposed structure of $[RuCl(AMBI)(H_2O)_3]Cl_2$ complex.

Table 1
Cyclic voltammetric data for the ruthenium(III) complex.

Complex	$E_{pa}(V)$	$E_{pc}(V)$	$\Delta E(V)$	$E_{½}(V)$	Assignment
$[RuCl(AMBI)(H_2O)_3]Cl_2$	–	−0.90	0.90	−0.45	Ru^{III}/Ru^{II}
	1.107	1.041	0.066	1.074	Ru^{III}/Ru^{IV}

Conditions: supporting electrolyte (0.2 g, TBHFP), the concentration of the complex; ~10–^{3} M, $\Delta E = E_{pa} - E_{pc}$ and $E_{1/2} = 0.5(E_{pa} + E_{pc})$, where E_{pa} and E_{pc} are the anodic and cathodic cyclic voltammetric peak potentials.

2.10.2. In vivo tumor cell transplantation

Ehrlich ascites carcinoma (EAC) cell line was obtained from the El-Nile Research Centre (El-Mansoura, Egypt), in a donor female mouse (Swiss Albino) of 19 g body weight. EAC cells in female mice are the model of mammary gland carcinoma, which similar to breast cancer in human [28]. The EAC cells were drawn from the intraperitoneal cavity by a sterile syringe, then washed three times with sterile saline then centrifuged. Then the pellets were suspended in sterile isotonic saline. The viability of the cells was 98% as judged by trypan blue exclusion assay.

The mice groups were divided into six groups (10 mice in each group) namely:

i) The control group: which injected with sterile distilled water for injection (the drug solvent) for twelve days;
ii) The EAC group: were injected with 100 μL (EAC suspension) containing 2.5×10^6 viable EAC cells;
iii) The treated group which injected I.P. with 2.5×10^6 viable EAC cells and after 2 h, injected intraperitoneally with different doses of Ru(III) complex and divided into: Low dose, 25 mg/kg, treated mice (I) and high dose, 50 mg/kg (1/4 LD_{50}), treated mice (II); for 12 days;
iv) The last two groups were healthy mice treated with 25 mg/kg and 50 mg/kg doses of Ru(III) complex for 12 days to improve its effect on normal mice, and named low dose group and high dose group.

At the end of the experiment and after fasting overnight; animals from each group were sacrificed, and the other animals were left till the day 14 for mortality percent calculations. After the day 14 all the live animals were sacrificed. Serum and blood samples were collected for the study of chemistry, antioxidant activities and hematological parameters. Liver samples from each group were washed with PBS buffer (pH 7.4) and immersed in the 10% formalin and sent for histopathological examination.

2.11. Quantitative RT-PCR analysis

RNA extraction from mice liver was done by Gene JET RNA Purification Kit (Thermo Scientific, # K0731, USA) according to the manufacturer's protocol. Total RNA (5 μg) was reverse transcribed using Revert Aid H Minus Reverse Transcriptase (Thermo Scientific, #EP0451, USA) to produce cDNA [29]. The cDNA was used as a template to determine the relative expression of the topoisomerase I (*TopI*) gene using Step One Plus real time PCR system (Applied Biosystem, USA). The primers were designed by Primer 5.0 software and their sequences were as follow: *TopI* F: 5′GAGACTGCGCGGCGTCTGAA3′ and *TopI* R: 5′ CAGCCCACAGTGTCTGCCGT3′. The housekeeping gene *GAPDH* (with primer sequences; F: 5′ TGTGTCCGTCGTGGATCTGA 3′ and R: 5′ CCTGCTTCACCACCTTCTTGA 3′) was used as a reference to calculate fold change in target gene expression. After few steps, the cycle threshold (Ct) values were calculated for target genes and the housekeeping gene, and relative gene expression was determined using 2^−ΔΔCt method [30].

2.12. Statistical analysis

All data were expressed as means ± standard deviation (SD). The statistical significance was evaluated by one-way ANOVA using SPSS 18.0 software. Values were considered statistically significant when $p \leq 0.05$.

3. Results and discussion

3.1. Characterization of $[RuCl(AMBI)(H_2O)_3]Cl_2$

The analytical data of water soluble $[RuCl(AMBI)(H_2O)_3]Cl_2$ complex (Fig. 1) indicated that the complex has 1:1 (metal:ligand)

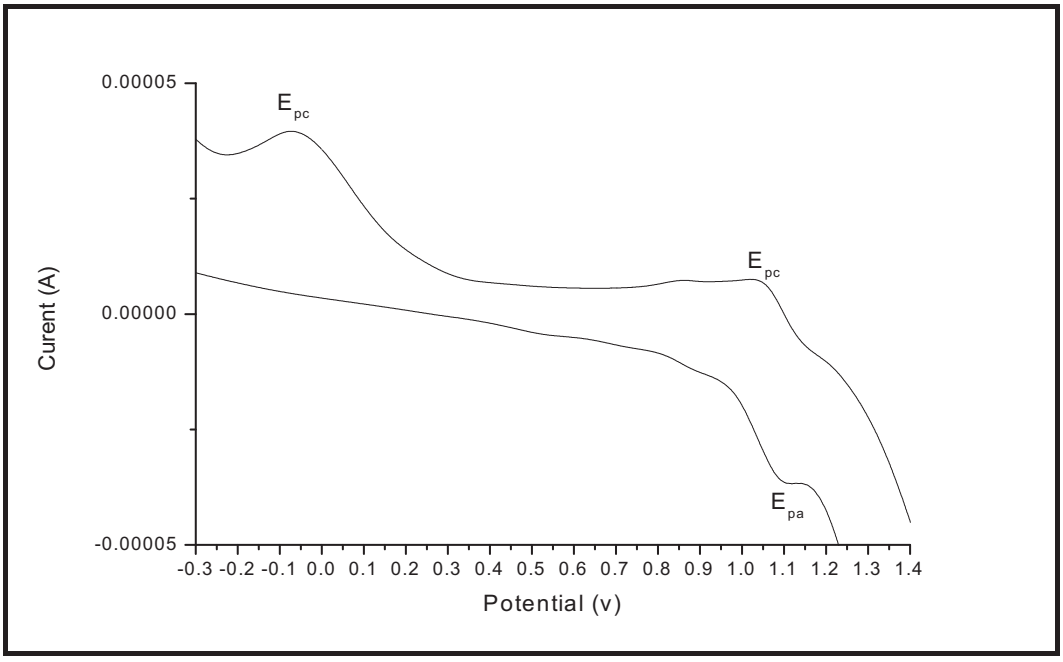

Fig. 2. Cyclic voltammogram of $[RuCl(AMBI)(H_2O)_3]Cl_2$.

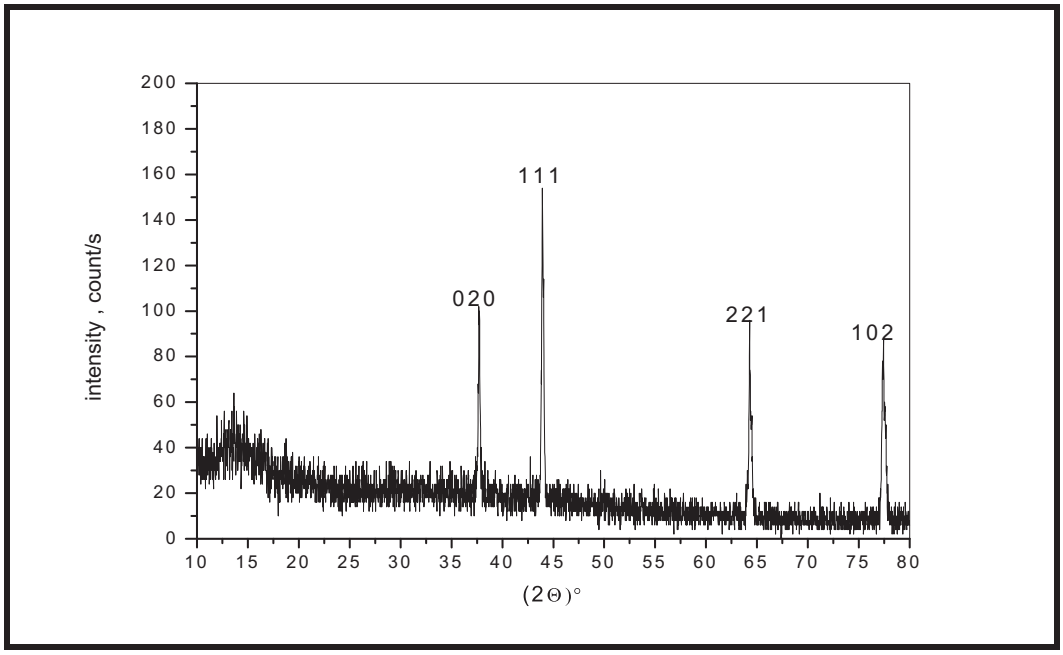

Fig. 3. XRD pattern for the powder of $[RuCl(AMBI)(H_2O)_3]Cl_2$.

stoichiometry. The molar conductance value for that complex (10^{-3} M H_2O) is 290 Ω^{-1} cm^2 mol^{-1} which indicating the electrolytic nature of the complex (presence of two chloride ions) [31]. The magnetic susceptibility measurement shows that the complex $[RuCl(AMBI)(H_2O)_3]Cl_2$ is paramagnetic ($\mu_{eff} = 1.82$ BM, low spin d^5 S = ½), as is normal for ruthenium(III) complex in an octahedral environment [4].

3.1.1. Infrared and electronic spectra of $[RuCl(AMBI)(H_2O)_3]Cl_2$

The infrared spectrum of the free (AMBI) ligand shows one medium and broad absorption band in the region 3338–3270 cm^{-1}, indicating the vibration of the tertiary nitrogen atom of imidazole ring ν(—N═CH—) and nitrogen atom of amino group $\nu(NH_2)$. This band was shifted toward lower frequency in the spectrum of Ru(III) complex (3220–3155 cm^{-1}). This indicates that coordination of the ligand (AMBI) to Ru(III) ion *via* the tertiary nitrogen atom of imidazole ring and nitrogen atom of amino group. These results are supported by the appearance of new weak band at about 440 cm^{-1} attributable to ν(Ru—N) stretching [32].

The electronic spectrum of Ru(III) complex was recorded in water solvent in the range of 200–700 nm. The ground state of Ru(III) in an octahedral environment is $^2T_{2g}$ and the first excited doublet levels in the order of increasing energy are $^2A_{2g}$ and $^2T_{1g}$, which arise from $t_{2g}^4 e_g^1$ configuration. These bands in the region 260–350 nm are assigned to π-π* and n-π* transitions, respectively. Beside these bands the spectrum showed a third intense absorption band at 497 nm which can be assigned to charge transfer transitions [32]. These results are found to be in conformity with the assignments made for similar Ru(III) complex.

3.1.2. Electrochemical properties of $[RuCl(AMBI)(H_2O)_3]Cl_2$

Electrochemical properties of this complex were investigated by cyclic voltammetry in DMF solvent (0.2 g TBHFP). Voltammetric data are presented in Table 1 and selective voltammogram is shown in Fig. 2. The voltammogram showed one irreversible reduction peak at −50 mV on the negative side against Ag^+/AgCl, and reversible oxidation wave (ΔE = 50 mV) on the positive side. The former is assigned to Ru^{III}/Ru^{II} reduction and the latter is assigned to Ru^{III}/Ru^{IV} oxidation. The one-electron nature of these waves can be established by comparing the peak heights for each wave with that of the ferrocene-ferrocenium couple under the same conditions. Similar results were reported for Ru^{III} complexes of octahedral environment [29].

3.1.3. X-ray diffraction analysis

The X-ray diffraction (XRD) pattern of the Ru(III) complex is shown in Fig. 3. The pattern of that complex shows a broad hump at 2Θ = 14° in addition to four sharp diffraction peaks at 2Θ of 37.7, 43.9, 64.3, 77.4°. This behavior indicate that the powder is a mixture of amorphous and polycrystalline phases [33]. The lattice crystal system and parameters which are a, b, c, α, β and γ for the complex are determined with using CRYSFIRE computer program [34]. The optimum indexed miller indices and space group are obtained using CHEKCELL program [35]. It is found that Ru(III) complex has an orthorhombic crystal system with space group PCCA. The obtained values of lattice parameters are 5.231, 4.774, 2.536, 90, 90 and 90 for a, b, c, α, β and γ, respectively. The determined crystallite size for complex is 37 nm.

3.1.4. Thermal analyses

The TGA curve of the complex shows that the change of substituent affects the thermal properties of complex. The temperature intervals and the percentage of loss of masses are listed in Table 2. Ru(III) complex shows four decomposition steps, the first stage occurs in the temperature range 30–200 °C is attributed to loss of two (Cl^-), the second stage in the temperature range 200–320 °C is attributed to loss of three molecules (H_2O), the third stage in the temperature range 320–420 °C corresponding to loss of a part of the complex ($C_8H_9N_3Cl$). The final weight loss is due to the ruthenium oxide residue [36].

Table 2
The thermal analyses data of $[RuCl(AMBI)(H_2O)_3]Cl_2$ complex.

Complex	Loss	Temp. range assignment (°C)	Calc. mass (found.) %
$[RuCl(AMBI)(H_2O)_3]Cl_2$	Cl_2	100–200	13.20 (13.01)
	$3H_2O$	200–320	17.35 (17.03)
	$C_8H_9N_3Cl$	320–420	44.62 (44.90)
	RuO_2	>500	24.71(24.99)

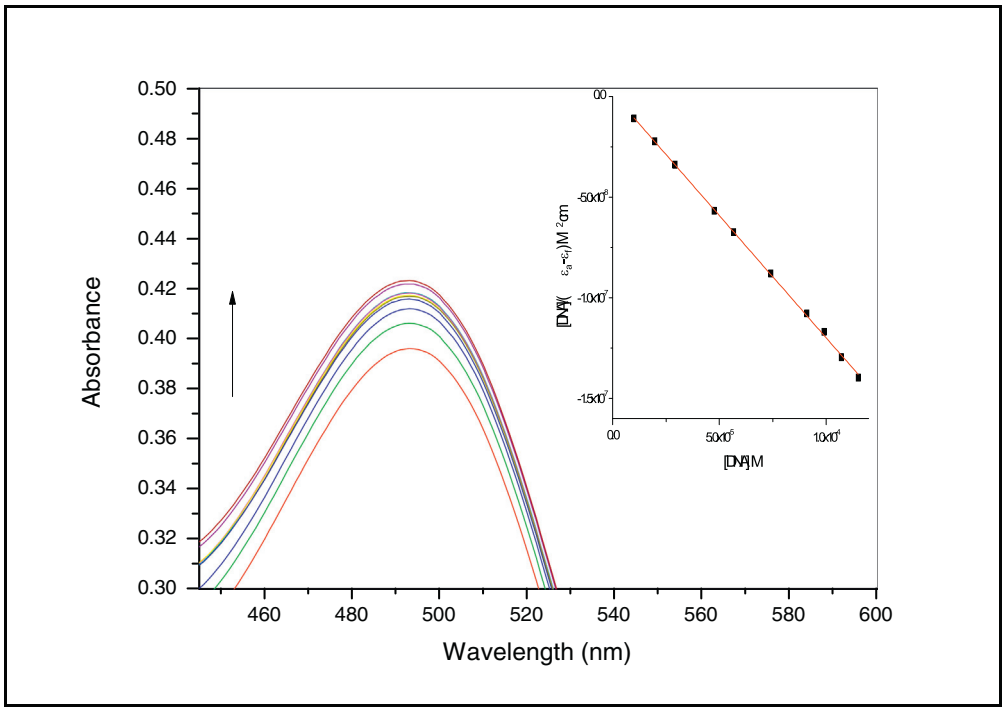

Fig. 4. Absorbance spectra of complex in buffer pH 7.2 at 25 °C in the presence of increasing amount of CT-DNA. Arrow indicates the changes in absorbance upon increasing CT-DNA concentration. Inset: plot of [DNA]/ $(\varepsilon_a - \varepsilon_f)$ M^2cm *vs.* [DNA] M for titration of DNA with complex. (For interpretation of the references to color in this figure, the reader is referred to the web version of this article.)

3.2. DNA binding studies

3.2.1. Electronic absorption studies

The intrinsic binding constant to CT-DNA by monitoring the absorption intensity of the charge transfer spectral band at 497 nm for the complex was determined by titration with UV spectrophotometry (Fig. 4). Upon the addition of increasing amounts of CT-DNA, a significant "hyperchromic" effect was observed accompanied by a moderate blue shift of 2–3 nm, indicating the stabilization of the DNA helix. These spectral characteristics suggest that the complex bind either to the external contact (electrostatic binding) or to the major and minor grooves of DNA. Hypochromism possibly results from the interaction between the electronic states of the intercalating chromophore and that of the DNA base [37]. Moreover, this "hyperchromic effect" can be explained based on the large surface area of the complex as well as presence of planar aromatic chromophore facilitates a strong binding interaction of the complex with CT-DNA *via*, partial insertion of the aromatic moiety in between the stacking base pair [38]. The intrinsic binding

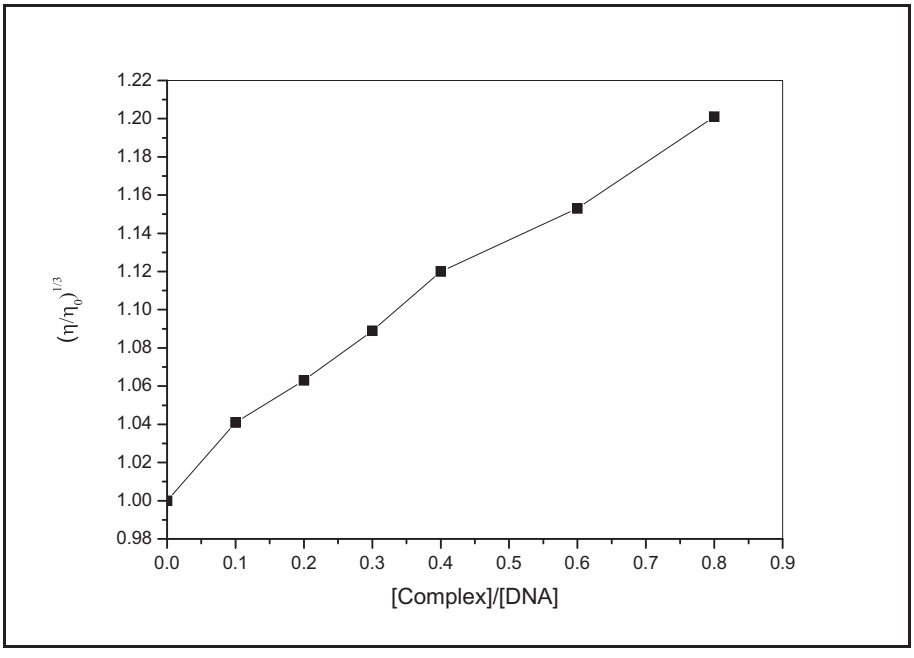

Fig. 5. Effect of increasing amounts of Ru(III) complex on the relative viscosity of CT-DNA (1×10^{-3} M) at 25 °C.

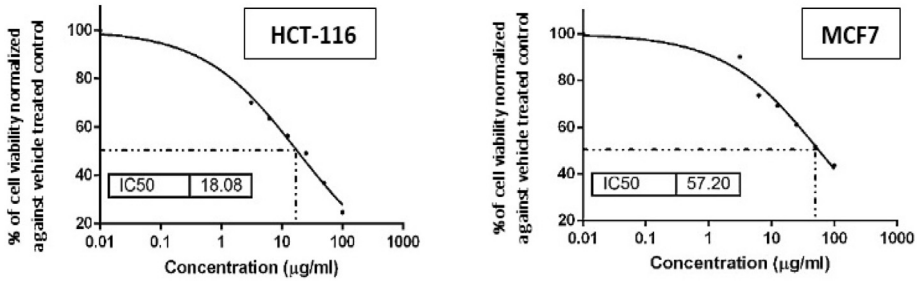

Fig. 6. The percent of cell inhibition diagram of the human colon carcinoma (HCT-116) and breast adenocarcinoma (MCF-7) cell lines against different concentration of Ru(III) complex.

constant (K_b) of the complex with CT-DNA was determined (Eq. (1)) and found to be 8.3×10^{-5}.

3.2.2. Viscosity determination

Viscosity measurements were proved to be less ambivalent to support a complex-DNA binding model, as these measurements are very much sensitive to the length change [39]. When a small molecule intercalates between the DNA base pairs, it unwinds the DNA helix and hence increases lengthen it, resulting in a significant increase in the viscosity of DNA solution. However, a partial and/or non-classical intercalation of ligand may bend the DNA helix, resulting in the decrease of its effective length and its viscosity [24]. The binding of the complex with CT-DNA was clarified by measuring the relative specific viscosity of DNA after the addition of varying concentration of the complex. To further investigate the interaction mode of the binding mode of complexes with DNA, a viscosity study was carried out at 25 °C (Fig. 5). Viscosity experimental results obviously showed that the relative viscosity of CT-DNA increases gradually by addition of increasing concentration of the complex. This observation can be explained in the fact that, classical intercalation model demands that the DNA helix must lengthen as base pairs are separated to accommodate the binding complexes, leading to the increase of DNA viscosity, as for the behaviors of the known DNA intercalators.

3.3. Anticancer activity of $[RuCl(AMBI)(H_2O)_3]Cl_2$

3.3.1. In vitro assay

Determination of anticancer activity against the human colon carcinoma (HCT-116) and breast adenocarcinoma (MCF-7) cell lines was done by MTT assay in the presence of cisplatin as a reference anticancer drug. The complex shows good cytotoxicity against the two cell lines with IC_{50} 18.08 and 57.20 μg/mL, respectively (Fig. 6); while the IC_{50} of cisplatin against these two cell lines was 18 and 22 μg/mL, respectively. These results showed the antiproliferative effect of Ru(III) complex on HCT-116 cells was nearly as the cisplatin value; that indicates its efficiency as anticancer agents. While, its IC_{50} on MCF-7 increased approximately two folds than the cisplatin value, that indicates lower toxicity of Ru(III) complex. The cytotoxic effect of Ru(III) complex increases with increasing dose in both MCF-7 and HCT-116 cell lines (Fig. 6), which also observed by Gozzi et al. [40] when the cytotoxicity of his ruthenium complex toward the two cell lines was by dose-dependent manner. Recent studies with different ruthenium complexes had confirmed the antiproliferative effect of these complexes against MCF-7 cell line [41–45] and against human colon carcinoma [46–48].

3.3.2. Evaluation of cell death mode

The cell death occurs by necrosis or apoptosis. When necrosis occurs; the cell loses its ions, organelle swell as well as the whole cell, then the membrane permeability increases with releasing the cell's intracellular content [49]. While, in apoptosis (programmed cell death) the cell shrinks, keeping the plasma membrane integrity, and nuclear destruction occurs [50]. *In vivo*, inflammation is engaged with necrotic cell death pathway not apoptotic one [51]. The injection of IC_{50} value of the $[RuCl(AMBI)(H_2O)_3]Cl_2$ into the cell lines before incubation for 24 h, then stained with the acridine orange/ethidium bromide to be visualized by their colors. Where, the vital cells appear green, the necrotic cells appear red and the apoptotic one appears yellow. The Ru(III) complex shows the apoptotic effect on both MCF-7 and HCT-116 cell lines by percent to 23.1 and 33.1%, while the necrotic percentage is very small (Fig. 7). Indicating that this complex may activate the natural cell death pathway and that will stop the proliferation of cancer cells. As shown in Fig. 7, the apoptosis (programmed cell death) was increased

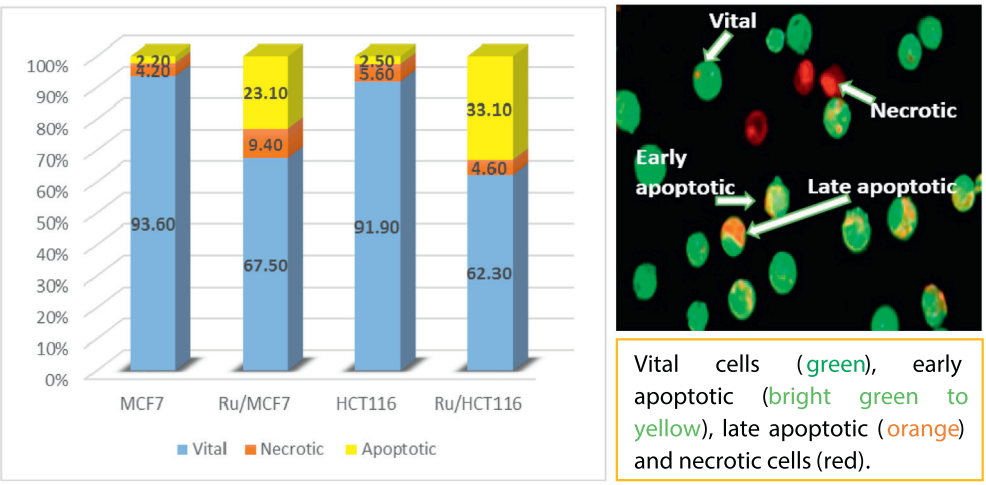

Fig. 7. In the left: The percent of apoptosis and necrosis cell death in both MCF-7 and HCT-116 treated cells compared to the control one. In the right: The fluorescence microscopy photo of the stained apoptotic and necrotic cells treated with the IC_{50} of the Ru(III) complex. (For interpretation of the references to color in this figure, the reader is referred to the web version of this article.)

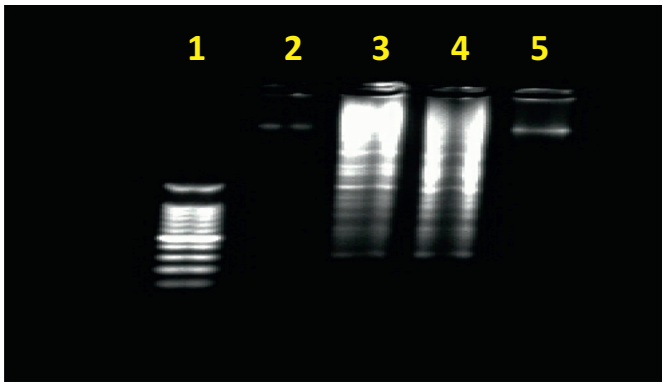

Fig. 8. The agarose gel for DNA damage assay. Lane 1: DNA ladder, lane 2: normal colon cancer cells, lane 3: treated colon cancer cells showed smears and fragmentation in the end of the lane. Lane 4: treated MCF-7 cells showed smears and fragmentation and lane 5: normal MCF-7 cells.

ten folds in the treated MCF-7 than its percentage in the absence of Ru (III) complex. That indicates the nuclear fragmentation of the cellular DNA content that may be due to the binding between our [RuCl (**AMBI**)$(H_2O)_3$]Cl_2 and the DNA. Also, in treated HCT-116 cell line the apoptotic percentage increases about thirteen times than its percent in cancer cells without treatment. Several studies supported our results of the apoptotic activation of ruthenium compounds on different cell lines [52,53]. However, the ruthenium compounds may have another way to destroy cancer cell besides apoptosis but needs more analysis to be confirmed.

3.4. DNA damage assay

The DNA ladder assay is a strong indicator of the apoptotic cell death [54]. The apoptotic appears as DNA ladder bands in the DNA samples. To confirm the apoptotic pathway of [RuCl(AMBI)$(H_2O)_3$]Cl_2 as anticancer agent, the DNA ladder assay by gel electrophoresis was done. When comparing the DNA fragmentation of the cancer cell line with the treated one in the presence of DNA ladder as a standard; we found that; the fragmentation bands of the treated cell line's DNA appear, and the DNA degraded into several bands. Fig. 8 showed that, in lane 3 and 4 there were DNA laddering in both MCF-7 and HCT-116 treated cells compared with untreated ones (lanes 2 and 5), respectively. These indicated the apoptotic cell death and a destruction in the nuclear DNA of the two cell lines when treated with our Ru(III) complex. This may due to the attack of the nuclear DNA by our Ru(III) complex and destroying it. These results agree with the previous DNA binding and apoptotic cell death results.

Otherwise, the smearing of the treated cell line's DNA indicated slightly necrosis. So, Ru(III) complex may take necrotic pathway, in smaller extent, besides the apoptotic one. To approve which pathway to be selected, we made the cell cycle analysis by flow cytometric technique.

3.5. Cell cycle analysis

The cell cycle (cell division) phases include gap 0 (G0), gap 1 (G1), gap 2 (G2) and synthesis (S) phases; then mitosis (M). Any percentage changes between these phases leads to cell cycle arrest. To indicate the mechanism of this compound as anticancer drug, a flow cytometric analysis was done on the treated HCT-116 and MCF-7 cell lines with the IC_{50} of the Ru(III) complex compared to the untreated one. Fig. 9 shows a decrease in S phase percent in treating MCF-7 cells by half fold, that indicates the decrease entrance of the cell into DNA synthesis phase and leads to decreased replication of cancer cells by the Ru(III) complex due to its interaction with the DNA. Also, the decrease in G0/G1 from 45% in untreated cells to 20% for the treated one; indicates decreased cell proliferation by treatment. In addition, there was an increase in G2/M in treating MCF-7 cells from 25% in untreated cells to 66% indicating the cell cycle arrest in this phase. This accumulation in G2/M indicates the interactions of the Ru(III) complex with DNA that prevents the entry of the cancer cells into a new cell cycle.

A similar effect of the Ru(III) complex on HCT-116 cell line, both percent of G0/G1 and S phase decreased in the treated cells than the control

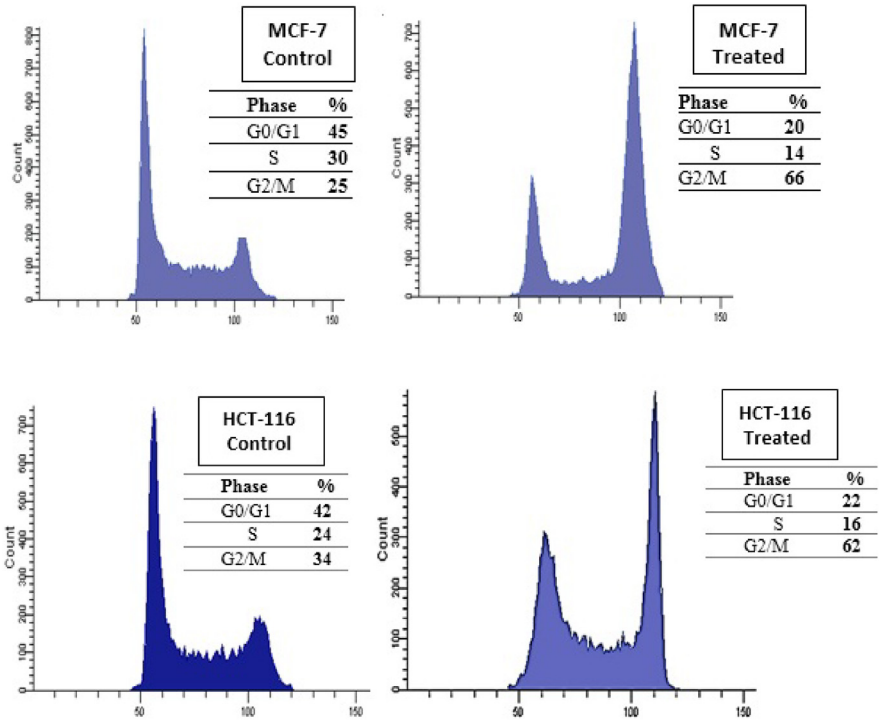

Fig. 9. Percent of MCF-7 and HCT-116 cells in different phases of cell cycle after treatment with IC_{50} of Ru(III) complex compared to untreated cells (control).

Table 3
Mean serum levels of liver and kidney functions tests.

Group	GOT U/L	GPT U/L	Albumin g/dL	Bilirubin mg/dL	Creatinine mg/dL	Urea mg/dL	Uric acid mg/dL
Control	145 ± 16.5	49 ± 10.7	2.9 ± 0.09	0.13 ± 0.1	0.57 ± 0.1	35.4 ± 1.4	2.85 ± 0.1
EAC	258 ± 50*	103 ± 11.9*	1.7 ± 0.15*	0.3 ± 0.07*	0.96 ± 0.1*	41.5 ± 1.3*	3.74 ± 0.1*
Low dose, 25 mg/kg, treated mice (I)	209 ± 45#	88 ± 6.1#	2.5 ± 0.1#	0.2 ± 0.08#	0.62 ± 0.1#	33.5 ± 1.9#	2.78 ± 0.2#
High dose, 50 mg/kg, treated mice (II)	215.8 ± 34a	99.9 ± 19a	2.35 ± 0.1#	0.18 ± 0.06#	0.82 ± 0.1a	33.4 ± 3.2#	2.84 ± 0.2#
Low dose group	178 ± 15*	86.5 ± 9.6*	2.8 ± 0.12b	0.15 ± 0.5b	0.62 ± 0.1*	36.7 ± 4.5b	2.87 ± 0.2b
High dose group	192 ± 16*	95 ± 4.4*	2.4 ± 0.12*	0.14 ± 0.5b	0.7 ± 0.04*	31.7 ± 3.6*	2.9 ± 0.14b

Values represent mean ± standard deviation.
* $p < 0.05$ compared to control group.
# $p < 0.05$, compared to EAC group.
a Non-significant $p > 0.05$, compared to EAC group.
b Non-significant $p > 0.05$, compared to control group.

cells, with an increased in the percent of a G2/M percent in the treated cells than the control one (Fig. 9).

3.6. In vivo experiment

EAC cells are a liquid tumor appears in the abdominal region, where the untreated mice will have a large abdominal size. In our study, the mean abdomen circumference of the EAC group, control and treated groups was 11.6, 7.9 and 8.4 cm, respectively. So, there is no significant increase in abdominal size of the treated groups when compared with the control one, this indicates that the EAC cell proliferation were stopped by the Ru(III) complex. Also, at the end of the experiment (14 days) all the EAC mice were dying while only one mouse from the low dose, 25 mg/kg, treated mice (I) was died; that confirms the anticancer effect of Ru(III) complex with lower toxicity.

After the end of the experiment; the biochemical parameters were analyzed in all groups. Serum glutamate-oxaloacetate transaminase (SGOT) and Serum glutamate-pyruvate transaminase (SGPT) are liver enzymes that produced in the hepatocytes and catalyze the transamination reactions in the amino acid metabolism. When liver injury, damage or cancer occurs, these enzymes were spilled out from the hepatocytes into the blood stream and their levels increased in plasma. The severity of liver damage is determined by the degree of elevation of these enzymes especially the SGPT. If enzymes levels were decreased again, this will be an indication of hepatocyte healing or repair. Table 3 shows that the SGOT and SGPT in low dose, 25 mg/kg, treated mice (I) was significantly decreased than EAC group but didn't reach the values of the control group. While, the albumin value of the low dose, 25 mg/kg, treated mice (I) was significantly increased than the EAC one. However, the bilirubin and creatinine levels in the low dose, 25 mg/kg, treated mice (I) was significantly decreased than their levels in EAC group and reaches the control group levels. Also, urea and uric acid levels in the low dose, 25 mg/kg, treated mice (I) were significantly decreased than their levels in EAC group and reaches the control group levels. To indicate the toxicity of this dose on healthy mice, the low dose group was done for 12 days. As listed in Table 3, the SGOT and SGPT levels in the low dose group were elevated than the control group, but still less than their levels in the EAC group. This may due to the slight toxicity of the Ru(III) complex on the hepatocytes, but this toxicity didn't cause severe liver injury as indicated from albumin results which is significantly increased than the EAC group and reaches its control level. Also, the bilirubin level didn't elevate in the low dose group. The creatinine level was slightly increased than the control group, but the urea and uric acid levels were not changed than the control group. These results indicated that the Ru(III) complex in that dose was toxic to cancer cells and safe on liver and kidney cells.

However, the creatinine level was elevated in high dose, 50 mg/kg, treated mice (II) than the control one, but, the urea and uric acid levels still in their normal levels which indicate slight injury of the kidney by high doses of the Ru(III) complex. On the other hand, the SGOT and SGPT in high dose, 50 mg/kg, treated mice (II) and in the high dose groups were elevated than the control group with slightly decrease in albumin levels in these groups than the control one, but still higher than those of the EAC group. Hence, Ru(III) complex hepatotoxicity was increased with high dose so, caution may be noticed in higher doses.

Since the main problem of cisplatin treatment is its nephrotoxicity [55]: our results show that the kidney function tests (creatinine, urea and uric acid) were decreased significantly in the treated group than the EAC group and reaches their value in the control one, that indicates the safety of our Ru(III) complex on the kidney. Another study established that the ruthenium complexes are safe on the kidney when the creatinine increases by 30% in treated mice, then decreased and reaches its normal value after 7 days of stopping the treatment [8] and the histological analysis of the kidney becomes normal after the first cycle of treatment, but the destruction of renal tubules appears after repeating the treatment cycles (these results are not found in our study). While in our study, there was slightly increased in creatinine value during the 12 day experiment (with decreased levels of other kidney function tests) which approved the safety of $[RuCl(AMBI)(H_2O)_3]Cl_2$ on the kidney.

3.6.1. Hematological parameters

The measuring of the red blood cells (RBCs) count indicates the oxidative damage to these cells which persuaded by the cancer. Also, the toxicity of the drug on the erythrocyte membrane can be predicted from the RBCs count. In our study, the effect of treatment with Ru(III)

Table 4
The hematological parameters in control, EAC, treated (I) and treated (II).

Group	Hb (g/dL)	RBCs ($\times 10^{12}$/L)	WBCs ($\times 10^{9}$/L)
Control	15.6 ± 0.4	8.70 ± 0.18	6.87 ± 0.43
EAC	10.4 ± 0.14*	5.59 ± 0.11*	11.10 ± 0.3*
Low dose, 25 mg/kg, treated mice (I)	12.2 ± 0.17#	6.00 ± 0.15#	7.30 ± 0.15#
High dose, 50 mg/kg, treated mice (II)	13.2 ± 0.11#	6.79 ± 0.22#	9.72 ± 0.14#
Low dose group	13.3 ± 0.23*	7.00 ± 0.13*	7.30 ± 0.2*
High dose group	13.4 ± 0.21*	7.40 ± 0.17*	8.10 ± 0.6*

Values represent mean ± standard deviation.
* $p < 0.05$ compared to control group.
# $p < 0.05$, compared to EAC group.

Table 5
Mean serum activities of SOD, CAT and TAC and the mean levels of GSH in serum and MDA in red blood cells.

Group	SOD U/mL	GSH U/L	Catalase (CAT) U/L	TAC mM/L	MDA/RBCs (mol/mL packed cells × 10^{-5})
Control	203.9 ± 9.6	198.4 ± 9.8	126.7 ± 4.1	1.5 ± 0.08	0.95 ± 0.13
EAC	118.7 ± 11.2*	82.9 ± 9.6*	68.5 ± 2.3*	0.83 ± 0.08*	2.9 ± 0.31*
Low dose, 25 mg/kg, treated mice (I)	238.5 ± 10.7#	180.6 ± 10#	107.3 ± 3.5#	1.3 ± 0.06#	1.7 ± 0.22#
High dose, 50 mg/kg, treated mice (II)	220.9 ± 11.9#	171 ± 7.9#	119.8 ± 6.5#	1.4 ± 0.04#	1.5 ± 0.28#
Low dose group	161 ± 8.6*	145.3 ± 5*	95 ± 4.6*	1.3 ± 0.08*	1.1 ± 0.1*
High dose group	186 ± 8.9*	176.7 ± 3.5*	92 ± 4.4*	1.3 ± 0.04*	1.3 ± 0.25*

Values represent mean ± standard deviation.
* $p < 0.05$ compared to control group.
\# $p < 0.05$, compared to EAC group.

complex in the low dose, 25 mg/kg, treated mice (I) and in high dose, 50 mg/kg, treated mice (II) was shown in Table 4: the hematological parameters were evaluated in comparison to EAC group. Our results show that, there is a statistically higher hemoglobin concentration (Hb) in low dose, 25 mg/kg, treated mice (I) and in high dose, 50 mg/kg, treated mice (II) in comparison to EAC group. Also, the RBCs count increased in low dose, 25 mg/kg, treated mice (I) and in high dose, 50 mg/kg, treated mice (II) when compared to EAC group. On the other hand, the leukocyte count increases significantly in the EAC group than the control group because of cancer cell replication that elevated the inflammation. As the treatment stops cancer cell's replication; the white blood cells (WBCs) count decreased in the low dose, 25 mg/kg, treated mice (I) and in high dose, 50 mg/kg, treated mice (II) when compared with the EAC group.

Also, to indicate the toxicity of our complex the hematological parameters were measured in the low and high doses groups. As the hemoglobin and RBCs levels were slightly decreased in these groups than the control group, but still higher than the EAC group, which indicated little toxicity on red blood cells. While the WBCs count in the low and high dose groups were slightly elevated than the control group because of the toxicity to the liver cells which leads to inflammation that increases the WBCs count. Similarly, the improvement of the hematological parameters in the treated groups than the EAC one indicates the safety of our Ru(III) complex. Also, the decreased in hemoglobin and RBCs count in the EAC group because the oxidative damage of the red cells by the free radicals; which eliminated by the treatment and appear in increasing the hemoglobin and RBCs count.

3.6.2. Mortality percentage/group

Mortality of the experimental mice was calculated at the end of the experiment (Eq. (5)) when the first EAC-mice was dying (after 12 days). 5 mice from each group were kept till the 14 days, 3 mice from 4 of the EAC group were dead on the 13th day and the last one died in the 14th day.

$$\text{Mortality percentage in a group } (\%\text{Mt}) = \frac{\text{Number of dead mice}}{\text{Total number of mice}} \times 100 \quad (5)$$

The mortality percentage (% Mt) of the treated group (I) was 10% compared with the control group. While, the % Mt of the treated group (II) was 20% in comparison with the control group. The % Mt of the EAC group was 100% at day 14.

3.6.3. Antioxidant activity assay

The reactive oxygen species (ROS) had a very high levels in cancer cells due to increased metabolic activity and cyclooxygenases [56]. ROS always damage tissues, organs and DNA [57]. Antioxidant enzyme's role is to scavenge different ROS, but when these ROS increases -by cancer- the activity of these enzymes was depleted. Superoxide dismutase (SOD) role is to scavenge superoxide anion and protect the cell from damage [58]. Catalase (CAT) can scavenge the intracellular hydrogen peroxide and reduces the oxidative cell damage [59]. Glutathione acts by reducing the disulphide bonds of cytoplasmic protein to cysteines. Glutathione reductase (GSH) reduces the oxidized glutathione into its reduced form and hence scavenge the present ROS [60]. The overall degree of oxidative damage was indicated by the level of malondialdehyde (MDA) [61].

It was shown from Table 5 that, the SOD levels in the EAC group were significantly decreased than the control one due to the healthy cell's damage accompanying the cancer burden. While, in the low dose, 25 mg/kg, treated mice (I) and high dose, 50 mg/kg, treated mice (II) the SOD levels were significantly increased than the EAC and the control ones. This can be due to cell damage accompanying the cancer burden reduction, and the SOD compensates the increased ROS generated from the former damaged cells. Also, both GSH and CAT were significantly decreased in the EAC group in comparison to the control one; while increased again in Ru(III) complex treated group but not reach the control values. These results improved the removal of cancer burden from the cells by the Ru(III) complex and the cells repaired its antioxidant system again. At the same time, the total antioxidant capacity (TAC) which is the overall values of oxidant capacity was decreased in EAC group when compared to control one and then significantly increased in Ru(III) complex treated group as the cell damage stopped by the treatment. On the other hand, the MDA levels in red blood cells increased significantly in EAC group as the oxidative stress increased - in comparison to the control and treated group. However, the MDA level were decreased in the Ru(III) complex treated group than the EAC group but still in higher values when compared with the control one. This may contribute to the cancer burden which was found in the treated cells that make the cell compensate the damage by more antioxidant enzyme secretion to repair the damaged cells. Therefore, the depletion of the antioxidant enzyme in the EAC group and increased its

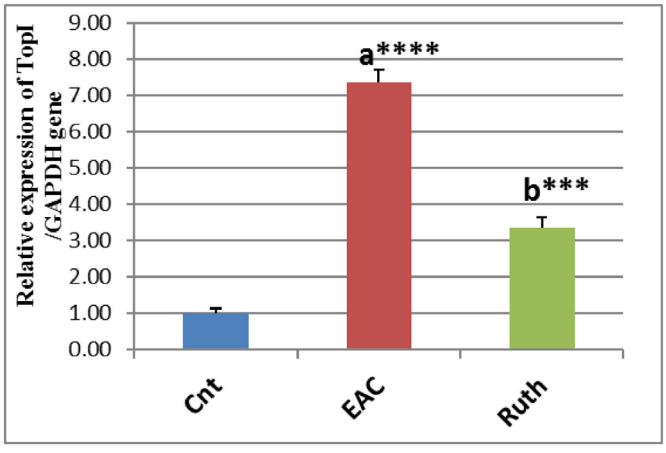

Fig. 10. Graphical presentation of real-time quantitative PCR analysis of the expression of *Top I* gene in liver of control (Cnt), Ehrlich Ascites Carcinoma (EAC), and Ru(III) complex treated group (I). Means within column carrying different superscript letters are significantly different (***$p \le 0.001$, ****$p \le 0.0001$).

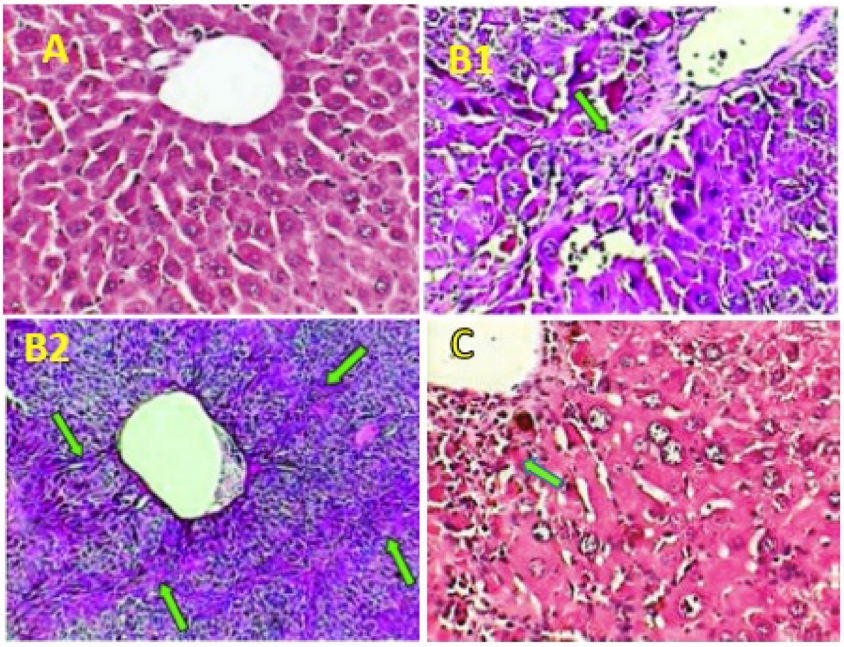

Fig. 11. Photomicrographs of liver sections: (A) normal control mice liver (×400) showing normal histological structure, (B1 (×400) and B2 (×100)) EAC mice liver sections showing severe damage of liver structure including the formation of pseudo lobules with fibrotic septa (green arrows) and (C) treated mice with 25 mg/kg liver section (×400) showing disarrangement of hepatic strands and few of fibrotic septa (green arrows). (For interpretation of the references to color in this figure legend, the reader is referred to the web version of this article.)

level in the treated groups proven the removal of the cancer burden by Ru(III) complex and reduction of the oxidative stress on the tissues. That makes us hypothesized that, Ru(III) complex have antioxidant characters or ROS scavenger; and this hypothesis were agreed with other studies [62,63].

3.7. Topoisomerase I assay

DNA is much longer than the organism itself (about 2 m long) then goes supercoiling process with compact several times to fit the cell nuclei (10^{-17} m^3). Topoisomerase I (*Top I*) can break the DNA double helix structure to allow relaxing of DNA for the transcription or replication processes [64]. *Top I* is an important enzyme that can be estimated in cancer cells [65] and the target enzyme for anticancer drugs [66]. Ruthenium complexes were found to inhibit topoisomerase I activity and be promising for anticancer therapy [67].

As shown in Fig. 10; the *Top I* activity was increased significantly in EAC group in comparison to control group, this may due to the highly proliferation of cancer cells than the normal one. On the other side, the *Top I* activity was half fold decrease in the low dose, 25 mg/kg, treated mice (I) than the EAC one and that may be due to the action of the Ru(III) complex as a topoisomerase I inhibitor which inhibit the replication of DNA in cancer cells and so the apoptosis process was increased. However, the *Top I* activity in the low dose, 25 mg/kg, treated mice (I) is still higher than that of the control one; because of the former cancer burden that was on the cells was stopped by the Ru(III) complex. Our results agreed with other study results that the *Top I* level was decreased in the treated group than the untreated one [68–70]. Which approved that our Ru(III) complex decreases cancer cell proliferation and hence the activity of *Top I* was decreased and blocks the DNA relaxation process, then stops the transcription/replication process of the cancer cells. Our result suggested that, our Ru(III) complex has an effects on DNA cleavage and forces the cancer cell toward the apoptotic pathway by decreased the *Top I* activity [71].

3.8. Histology results

The liver histopathological results are represented in Fig. 11. The liver sections of EAC induced mice (EAC group) showing hepatic nodules surrounded with mononuclear cells infiltration mostly surrounded with halo zone of suspected EACs, and most of hepatocytes were markedly vacuolated. While, the low dose, 25 mg/kg, treated mice (I) has a few fibrotic septa due to the Ehrlich cancer burden on the liver, but majority of liver cells is normal when compared with control and EAC groups. Another evidence of removing the cancer burden with minor hepatotoxicity is the histopathology; which improved that the low dose, 25 mg/kg, treated mice (I) liver affected a little by the treatment as most of its cells remain normal.

4. Conclusion

Synthesis and characterization of water soluble $[RuCl(AMBI)(H_2O)_3]Cl_2$ complex was described by different spectroscopic techniques. The molar conductance measurements proved that the complex is electrolyte. The CT-DNA binding activity of complex was studied by absorption spectra and viscosity measurements. Water soluble Ru(III) complex was promising chemotherapeutic drug against cancer both *in vitro* -by increasing the cell apoptosis and cell cycle arrest- and *in vivo* by stopping the EAC cells proliferation. It can be used in pre-clinical trials without worrying of nephrotoxicity, but care must be noticed about its liver toxicity. Also, more experiments must be done on different animal cancer models with the analysis of the molecular signaling pathway to prove the exact anticancer pathway of this compound.

Conflicts of interest

The authors declare no conflict of interest.

References

[1] E.P. Winer, Breast Cancer, Asco. 2015 Abstract https://doi.org/10.1093/med/9780199363315.003.0020.

[2] D. Hanahan, R.A. Weinberg, The hallmarks of cancer, Cell 100 (2000) 57–70, https://doi.org/10.1016/S0092-8674(00)81683-9.

[3] G. Giaccone, Clinical perspectives on platinum resistance, Drugs 59 (Suppl. 4) (2000) 9-17–8 http://www.ncbi.nlm.nih.gov/pubmed/10864226.

[4] A.F. Shoair, A.E.B. El-Bindary, M.K. Abd El-Kader, Structural and catalytic properties of some azo-rhodanine ruthenium(III) complexes, J. Mol. Struct. 1143 (2017) 100–115, https://doi.org/10.1016/j.molstruc.2017.03.109.

[5] M.J. Clarke, F. Zhu, D.R. Frasca, Non-platinum chemotherapeutic metallopharmaceuticals, Chem. Rev. 99 (1999) 2511–2534http://www.ncbi.nlm.nih.gov/pubmed/11749489.

[6] C. Mu, S.W. Chang, K.E. Prosser, A.W.Y. Leung, S. Santacruz, T. Jang, J.R. Thompson, D. T.T. Yapp, J.J. Warren, M.B. Bally, T.V. Beischlag, C.J. Walsby, Induction of cytotoxicity in pyridine analogues of the anti-metastatic Ru(III) complex NAMI-A by ferrocene functionalization, Inorg. Chem. 55 (2016) 177–190, https://doi.org/10.1021/acs.inorgchem.5b02109.

[7] M.I. Webb, C.J. Walsby, Albumin binding and ligand-exchange processes of the Ru (III) anticancer agent NAMI-A and its bis-DMSO analogue determined by ENDOR spectroscopy, Dalton Trans. 44 (2015) 17482–17493, https://doi.org/10.1039/c5dt02021b.

[8] M. Vadori, S. Pacor, F. Vita, S. Zorzet, M. Cocchietto, G. Sava, Features and full reversibility of the renal toxicity of the ruthenium-based drug NAMI-A in mice, J. Inorg. Biochem. 118 (2013) 21–27, https://doi.org/10.1016/j.jinorgbio.2012.09.018.

[9] M. Naseripour, R. Jaberi, A. Sedaghat, Z. Azma, M. Nojomi, K.G. Falavarjani, H. Nazari, Ruthenium-106 brachytherapy for thick uveal melanoma: reappraisal of apex and base dose radiation and dose rate, J. Contemp. Brachyther. 8 (2016)https://doi.org/10.5114/jcb.2016.57818.

[10] S. Kaliki, C.L. Shields, Uveal melanoma: relatively rare but deadly cancer, Eye 31 (2017)https://doi.org/10.1038/eye.2016.275.

[11] K. Hongthong, A. Ratanaphan, BRCA1-associated triple-negative breast cancer and potential treatment for ruthenium-based compounds, Curr. Cancer Drug Targets 16 (2016)https://doi.org/10.2174/1568009616666160203113957.

[12] A. Bergamo, A. Masi, M.A. Jakupec, B.K. Keppler, G. Sava, Inhibitory effects of the ruthenium complex KP1019 in models of mammary cancer cell migration and invasion, Met. Based. Drugs. 2009 (2009)https://doi.org/10.1155/2009/681270.

[13] D. Song, S. Ma, Recent development of benzimidazole-containing antibacterial agents, ChemMedChem 11 (2016) 646–659, https://doi.org/10.1002/cmdc.201600041.

[14] S.O. Podunavac-kuzmanovi, D.M. Cvetkovi, L.S. Vojinovi, Synthesis, physico-chemical characterization and biological activity of 2-aminobenzimidazole complexes with different metal ions, Apteff. (35) (2004) 239–246.

[15] C. Rajarajeswari, M. Ganeshpandian, M. Palaniandavar, A. Riyasdeen, M.A. Akbarsha, Mixed ligand copper(II) complexes of 1,10-phenanthroline with tridentate phenolate/pyridyl/(benz)imidazolyl Schiff base ligands: covalent vs non-covalent DNA binding, DNA cleavage and cytotoxicity, J. Inorg. Biochem. 140 (2014) 255–258, https://doi.org/10.1016/j.jinorgbio.2014.07.016.

[16] G. Kumaravel, P.P. Utthra, N. Raman, DNA fastening and scission actions of Cu(II), Co (II), Ni(II) and Zn(II) complexes: synthesis, spectral characterization and cytotoxic study, Appl. Organomet. Chem. (2017)https://doi.org/10.1002/aoc.4010.

[17] P. Peng, J.F. Xiong, G.Z. Mo, J.L. Zheng, R.H. Chen, X.Y. Chen, Z.Y. Wang, A concise synthesis of benzimidazoles via the microwave-assisted one-pot batch reaction of amino acids up to a 10-g scale, Amino Acids 46 (2014) 2427–2433, https://doi.org/10.1007/s00726-014-1794-z.

[18] C. Baik, W.S. Han, Y. Kang, S.O. Kang, J. Ko, Synthesis and photophysical properties of luminescent platinum(II) complexes with terdentate polypyridine ligands: [Pt (bpqb)X] and [Pt(tbbpqpy)X](PF6) (bpqb-H = 1,3-bis(4′-phenyl-2′-quinolinyl) benzene; tbbpqpy = 4-tert-butyl-1,3-bis(4′-phenyl-2′-quinolin)), J. Organomet. Chem. 691 (2006) 5912–5922, https://doi.org/10.1016/j.jorganchem.2006.09.062.

[19] L. Srikanth, V. Varun Raj, N. Raghunandan, L. Venkateshwerlu, Recent advances and potential pharmacological activities of benzimidazole derivatives, Der. Pharm. Chem. 3 (2011) 172–193.

[20] S. Velumani, X. Mathew, P.J. Sebastian, Structural and optical characterization of hot wall deposited CdSexTe1-x films, Sol. Energy Mater. Sol. Cells 76 (2003) 359–368, https://doi.org/10.1016/S0927-0248(02)00288-X.

[21] M.J. Waring, Complex formation between ethidium bromide and nucleic acids, J. Mol. Biol. 13 (1965) 269–282, https://doi.org/10.1016/S0022-2836(65)80096-1.

[22] M.E. Reichmann, S.A. Rice, C.A. Thomas, P. Doty, A further examination of the molecular weight and size of desoxypentose nucleic acid, J. Am. Chem. Soc. 76 (1954) 3047–3053, https://doi.org/10.1021/ja01640a067.

[23] A. Wolfe, G.H. Shimer, T. Meehan, Polycyclic aromatic hydrocarbons physically intercalate into duplex regions of denatured DNA, Biochemistry 26 (1987) 6392–6396, https://doi.org/10.1021/bi00394a013.

[24] S. Satyanarayana, J.C. Dabrowiak, J.B. Chaires, Tris(phenanthroline)ruthenium(II) enantiomer interactions with DNA: mode and specificity of binding, Biochemistry 32 (1993) 2573–2584, https://doi.org/10.1021/bi00061a015.

[25] M. Eriksson, M. Leijon, C. Hiort, B. Norden, A. Graeslund, Binding of .DELTA.- and .LAMBDA.-[Ru(phen)3]2+ to [d(CGCGATCGCG)]2 studied by NMR, Biochemistry 33 (1994) 5031–5040, https://doi.org/10.1021/bi00183a005.

[26] Y. Xiong, X. He, X. Zou, J. Wu, X. Chen, L. Ji, R. Li, J. Zhou, K. Yu, Interaction of polypyridyl ruthenium(II) complexes containing non-planar ligands with DNA, J. Chem. Soc. Dalt. Trans. (1999) 19–23, https://doi.org/10.1039/a806170j.

[27] D. Ribble, N.B. Goldstein, D.A. Norris, Y.G. Shellman, A simple technique for quantifying apoptosis in 96-well plates, BMC Biotechnol. 5 (2005) 12, https://doi.org/10.1186/1472-6750-5-12.

[28] P. Ehlich, Eperimentelle carcinomstudien na Mäusen, Arb. Inst. Exp. Ther. Frakfurt. 1 (1906) 78–80.

[29] M.A. El-Magd, H.E. Abbas, A.M. El-kattawy, A. Mokhbatly, Novel polymorphisms of the IGF1R gene and their association with average daily gain in Egyptian buffalo (*Bubalus bubalis*), Domest. Anim. Endocrinol. 45 (2013) 105–110, https://doi.org/10.1016/j.domaniend.2013.06.004.

[30] K.J. Livak, T.D. Schmittgen, Analysis of relative gene expression data using real-time quantitative PCR and the 2(−Delta Delta C(T)) method, Methods 25 (2001) 402–408, https://doi.org/10.1006/meth.2001.1262.

[31] W.P. Griffith, B. Reddy, A.G.F. Shoair, M. Suriaatmaja, A.J.P. White, D.J. Williams, Ruthenate(VI)-catalysed dehydrogenation of primary amines to nitriles, and crystal structures of cis-[Ru(bipy)2(NH2CH2Ph)2][PF6]2·0.5MeOH and cis-[Ru(bipy)2(NCPh)2][PF6]2·CH2Cl2 †, J. Chem. Soc. Dalt. Trans. 2 (1998) 2819–2826, https://doi.org/10.1039/a804071k.

[32] I.R. Baird, B.O. Patrick, K.A. Skov, B.R. James, Ruthenium(III and II) β-diketonate complexes containing imidazoles, Inorg. Chim. Acta. 466 (2017) 565–577, https://doi.org/10.1016/j.ica.2017.07.016.

[33] K.E. Lee, M. Wang, E.J. Kim, S.H. Hahn, Structural, electrical and optical properties of sol-gel AZO thin films, Curr. Appl. Phys. 9 (2009) 683–687, https://doi.org/10.1016/j.cap.2008.06.006.

[34] R. Shirley, The CRYSFIRE System for Automatic Powder Indexing, CRYSFIRE Syst. Autom. Powder Index, 2006.

[35] J. Laugier, B. Bochu, LMGP-Suite Suite of Programs for the Interpretation of X-ray Experiments, ENSP/Laboratoire Des Matériaux Du Génie Phys, BP 46. 38042 Saint Martin d'Hères, Fr, 2000 http://www.ccp14.ac.uk/tutorial/lmgp/ (Google Scholar).

[36] M. Hollering, M. Albrecht, F.E. Kühn, Bonding and catalytic application of ruthenium N-heterocyclic carbene complexes featuring triazole, triazolylidene, and imidazolylidene ligands, Organometallics 35 (2016) 2980–2986, https://doi.org/10.1021/acs.organomet.6b00504.

[37] B. Peng, Z. Gao, X. Li, T. Li, G. Chen, M. Zhou, J. Zhang, DNA binding, DNA cleavage and HSA interaction of several metal complexes containing N-(2-hydroxyethyl)-N′-benzoylthiourea and 1,10-phenanthroline ligands, JBIC J. Biol. Inorg. Chem. 21 (2016) 903–916, https://doi.org/10.1007/s00775-016-1388-1.

[38] J.P. Costes, F. Dahan, J.P. Laurent, M. Drillon, An alternating copper(II) chain with bridging oxamidato and nitrito ligands: crystal structure and magnetic properties of [Cu(NO2)2CuL]n(L═N,N′-bis(2-methyl-2-aminopropyl) oxamide), Inorganica Chim. Acta. 294 (1999) 8–13, https://doi.org/10.1016/S0020-1693(99)00223-6.

[39] V.G. Vaidyanathan, B.U. Nair, Oxidative cleavage of DNA by tridentate copper (II) complex, J. Inorg. Biochem. 93 (2003) 271–276, https://doi.org/10.1016/S0162-0134(02)00593-7.

[40] M. Gozzi, B. Schwarze, M.-B. Sárosi, P. Lönnecke, D. Drača, D. Maksimović-Ivanić, S. Mijatović, E. Hey-Hawkins, Antiproliferative activity of (η^6-arene)ruthenacarborane sandwich complexes against HCT116 and MCF7 cell lines, Dalton Trans. 46 (2017) https://doi.org/10.1039/c7dt02027a.

[41] P. Ramadevi, R. Singh, S.S. Jana, R. Devkar, D. Chakraborty, Mixed ligand ruthenium arene complexes containing N-ferrocenyl amino acids: biomolecular interactions and cytotoxicity against MCF7 cell line, J. Organomet. Chem. 833 (2017)https://doi.org/10.1016/j.jorganchem.2017.01.020.

[42] J. Lopes, D. Alves, T.S. Morais, P.J. Costa, M.F.M. Piedade, F. Marques, M.J. Villa de Brito, M. Helena Garcia, New copper(I) and heteronuclear copper(I)–ruthenium (II) complexes: synthesis, structural characterization and cytotoxicity, J. Inorg. Biochem. 169 (2017) 68–78, https://doi.org/10.1016/j.jinorgbio.2017.01.007.

[43] M. Płotek, R. Starosta, U.K. Komarnicka, A. Skórska-Stania, P. Kołoczek, A. Kyzioł, Ruthenium(II) piano stool coordination compounds with aminomethylphosphanes: synthesis, characterisation and preliminary biological study in vitro, J. Inorg. Biochem. 170 (2017)https://doi.org/10.1016/j.jinorgbio.2017.02.017.

[44] J.M. Gichumbi, B. Omondi, G. Lazarus, M. Singh, N. Shaikh, H.Y. Chenia, H.B. Friedrich, Influence of halogen substitution in the ligand sphere on the antitumor and antibacterial activity of half-sandwich ruthenium(II) complexes [RuX(η6-arene)(C5H4N—2—CH═N—Ar)]+, Zeitschrift Fur Anorg. Und Allg. Chemie. 643 (2017) 699–711, https://doi.org/10.1002/zaac.201600427.

[45] O.A. Lenis-Rojas, C. Roma-Rodrigues, A.R. Fernandes, F. Marques, D. Pérez-Fernández, J. Guerra-Varela, L. Sánchez, D. Vázquez-García, M. López-Torres, A. Fernández, J.J. Fernández, Dinuclear Ru^{II}(bipy)<inf>2</inf> derivatives: structural, biological, and in vivo zebrafish toxicity evaluation, Inorg. Chem. 56 (2017) https://doi.org/10.1021/acs.inorgchem.7b00790.

[46] P.R. Florindo, D.M. Pereira, P.M. Borralho, C.M.P. Rodrigues, M.F.M. Piedade, A.C. Fernandes, Cyclopentadienyl-ruthenium(II) and iron(II) organometallic compounds with carbohydrate derivative ligands as good colorectal anticancer agents, J. Med. Chem. 58 (2015) 4339–4347, https://doi.org/10.1021/acs.jmedchem.5b00403.

[47] Z. Ude, I. Romero-Canelón, B. Twamley, D. Fitzgerald Hughes, P.J. Sadler, C.J. Marmion, A novel dual-functioning ruthenium(II)-arene complex of an anti-microbial ciprofloxacin derivative - anti-proliferative and anti-microbial activity, J. Inorg. Biochem. 160 (2016) 210–217, https://doi.org/10.1016/j.jinorgbio.2016.02.018.

[48] P. Heffeter, A. Riabtseva, Y. Senkiv, C.R. Kowol, W. Körner, U. Jungwith, N. Mitina, B.K. Keppler, T. Konstantinova, I. Yanchuk, R. Stoika, A. Zaichenko, W. Berger, Nanoformulation improves activity of the (pre)clinical anticancer ruthenium complex KP1019, J. Biomed. Nanotechnol. 10 (2014) 877–884, https://doi.org/10.1166/jbn.2014.1763.

[49] J.F. Tait, Imaging of apoptosis, J. Nucl. Med. 49 (2008) 1573–1576, https://doi.org/10.2967/jnumed.108.052803.

[50] J.J. Lemasters, T. Qian, C.A. Bradham, D.A. Brenner, W.E. Cascio, L.C. Trost, Y. Nishimura, A.L. Nieminen, B. Herman, Mitochondrial dysfunction in the

pathogenesis of necrotic and apoptotic cell death, J. Bioenerg. Biomembr. 31 (1999) 305–319, https://doi.org/10.1023/A:1005419617371.
[51] S.Y. Proskuryakov, V.L. Gabai, Mechanisms of tumor cell necrosis, Curr. Pharm. Des. 16 (2010) 56–68, https://doi.org/10.2174/138161210789941793.
[52] D.G. Xing, Y. Zhang, G.J. Lin, Y.Y. Xie, S.Y. Deng, H.L. Huang, G. Bin Jiang, Y.J. Liu, In vitro cytotoxicity, cell cycle arrest, and antioxidation studies of ruthenium(II) complex [Ru(dmb)2(AHPIP)](ClO4)2, Med. Chem. Res. 23 (2014) 4376–4382, https://doi.org/10.1007/s00044-014-1000-6.
[53] M. Li, L. Lai, Z. Zhao, T. Chen, Aquation is a crucial activation step for anticancer action of ruthenium(II) polypyridyl complexes to trigger cancer cell apoptosis, Chem. Asian J. 11 (2016) 310–320, https://doi.org/10.1002/asia.201501048.
[54] Y. Gavrieli, Y. Sherman, S.A. Ben-Sasson, Identification of programmed cell death in situ via specific labeling of nuclear DNA fragmentation, J. Cell Biol. 119 (1992) 493–501, https://doi.org/10.1083/jcb.119.3.493.
[55] R.P. Miller, R.K. Tadagavadi, G. Ramesh, W.B. Reeves, Mechanisms of cisplatin nephrotoxicity, Toxins (Basel) 2 (2010) 2490–2518, https://doi.org/10.3390/toxins2112490.
[56] P. Storz, Reactive oxygen species in tumor progression, Front. Biosci. 10 (2005) 1881–1896 (doi:1667 [pii]).
[57] M. Dizdaroglu, P. Jaruga, Mechanisms of free radical-induced damage to DNA, Free Radic. Res. 46 (2012) 382–419, https://doi.org/10.3109/10715762.2011.653969.
[58] S.I. Liochev, I. Fridovich, The effects of superoxide dismutase on H_2O_2 formation, Free Radic. Biol. Med. 42 (2007) 1465–1469, https://doi.org/10.1016/j.freeradbiomed.2007.02.015.
[59] E. Nagababu, F.J. Chrest, J.M. Rifkind, Hydrogen-peroxide-induced heme degradation in red blood cells: the protective roles of catalase and glutathione peroxidase, Biochim. Biophys. Acta 1620 (2003) 211–217, https://doi.org/10.1016/S0304-4165(02)00537-8.
[60] N. Couto, J. Wood, J. Barber, The role of glutathione reductase and related enzymes on cellular redox homoeostasis network, Free Radic. Biol. Med. 95 (2016) 27–42, https://doi.org/10.1016/j.freeradbiomed.2016.02.028.
[61] L.J. Marnett, Lipid peroxidation-DNA damage by malondialdehyde, Mutat. Res. 424 (1999) 83–95, https://doi.org/10.1016/S0027-5107(99)00010-X.
[62] A.G.F. Shoair, E.-S.A. Toson, H.A. El-mezayen, Synthesis, spectral characterization and anticancer studies of three novel ruthenium(III) 2,2′-bipyridine complexes, Appl. Organomet. Chem. 29 (2015) 412–418, https://doi.org/10.1002/aoc.3307.
[63] C. Griffith, A.S. Dayoub, T. Jaranatne, N. Alatrash, A. Mohamedi, K. Abayan, Z.S. Breitbach, D.W. Armstrong, F.M. Macdonnell, Cellular and cell-free studies of catalytic DNA cleavage by ruthenium polypyridyl complexes containing redox-active intercalating ligands, Chem. Sci. 8 (2017)https://doi.org/10.1039/c6sc04094b.
[64] L. Stewart, M.R. Redinbo, X. Qiu, W.G. Hol, J.J. Champoux, A model for the mechanism of human topoisomerase I, Science 279 (1998) 1534–1541, https://doi.org/10.1126/science.279.5356.1534.
[65] F.W.A. Barros, D.P. Bezerra, P.M.P. Ferreira, B.C. Cavalcanti, T.G. Silva, M.G.R. Pitta, M. do C.A. de Lima, S.L. Galdino, I. da R. Pitta, L.V. Costa-Lotufo, M.O. Moraes, R.R. Burbano, T.N. Guecheva, J.A.P. Henriques, C. Pessoa, Inhibition of DNA topoisomerase I activity and induction of apoptosis by thiazacridine derivatives, Toxicol. Appl. Pharmacol. 268 (2013) 37–46, https://doi.org/10.1016/j.taap.2013.01.010.
[66] Y. Pommier, Topoisomerase I inhibitors: camptothecins and beyond, Nat. Rev. Cancer 6 (2006) 789–802, https://doi.org/10.1038/nrc1977.
[67] R.A. De Grandis, M.S. de Camargo, M.M. da Silva, É.O. Lopes, E.C. Padilha, F.A. Resende, R.G. Peccinini, F.R. Pavan, A. Desideri, A.A. Batista, E.A. Varanda, Human topoisomerase inhibition and DNA/BSA binding of Ru(II)–SCAR complexes as potential anticancer candidates for oral application, Biometals 30 (2017) 321–334, https://doi.org/10.1007/s10534-017-0008-z.
[68] X. He, L. Jin, L. Tan, DNA-binding, topoisomerases i and II inhibition and in vitro cytotoxicity of ruthenium(II) polypyridyl complexes: [Ru(dppz)2L]2+ (L = dppz-11-CO2Me and dppz), Spectrochim. Acta A Mol. Biomol. Spectrosc. 135 (2015) 101–109, https://doi.org/10.1016/j.saa.2014.06.147.
[69] X.W. Liu, S.B. Zhang, L. Li, Y.D. Chen, J.L. Lu, Ruthenium (II) complexes containing a new asymmetric ligand: DNA interaction, photocleavage and topoisomerase i inhibition, J. Organomet. Chem. 729 (2013) 1–8, https://doi.org/10.1016/j.jorganchem.2013.01.007.
[70] G. Liao, X. Chen, J. Wu, C. Qian, Y. Wang, L. Ji, H. Chao, Ruthenium(II) polypyridyl complexes as dual inhibitors of telomerase and topoisomerase, Dalton Trans. 44 (2015) 15145–15156, https://doi.org/10.1039/c4dt03585b.
[71] Y. Pommier, DNA topoisomerase I inhibitors: chemistry, biology, and interfacial inhibition, Chem. Rev. 109 (2009) 2894–2902, https://doi.org/10.1021/cr900097c.